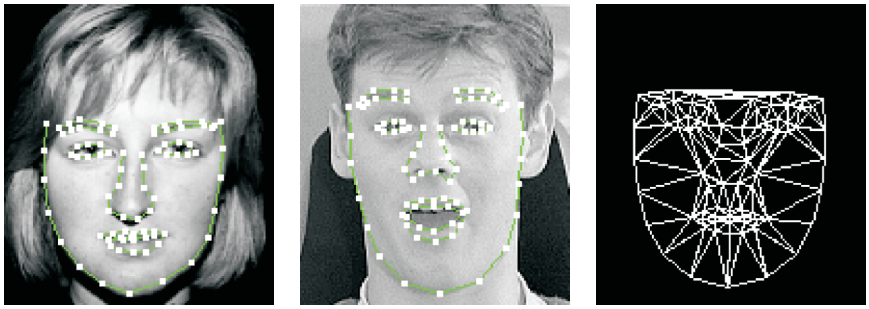

Figure 1. Two face instances labeled with 83 landmarks and the mesh of the mean shape. Reprinted with permission from SC Yan, C Liu, SZ Li, HJ Zhang, H Shum, QS Cheng. 2003. Face alignment using texture-constrained active shape models. *Image Vision Comput* **21**(1):69–75. Copyright ©2003, Elsevier.

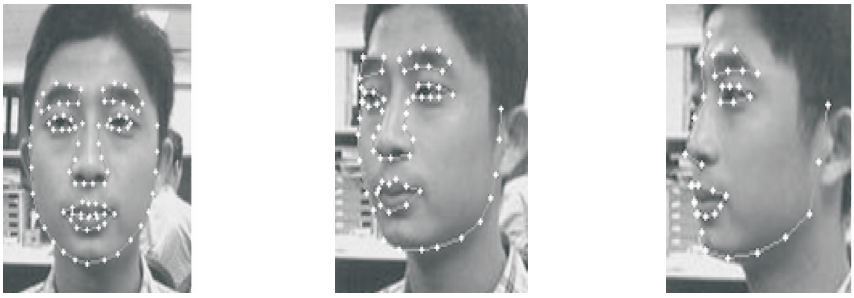

Figure 2. Frontal, half-side, and full-side view faces and the labeled landmark points. Reprinted with permission from SZ Li, SC Yan, HJ Zhang, QS Cheng. 2002. Multi-view face alignment using direct appearance models. *Proc 5th Int Conf Automatic Face Gesture Recogn*, pp. 309– 314. Copyright ©2002, IEEE.

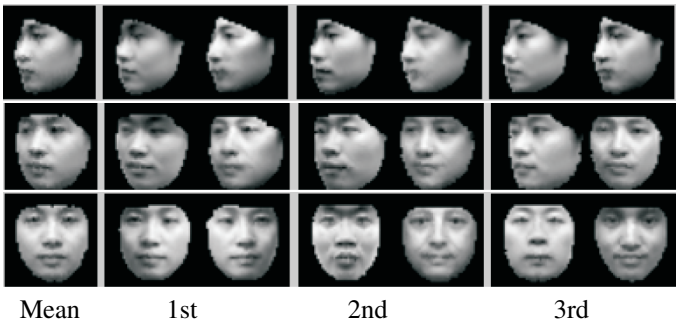

Figure 3. Texture and shape variations due to variations in the first three principal components of the texture (the shapes change in accordance with $s = \mathbf{R}t$) for full-side ($\pm 1\sigma$), half-side ($\pm 2\sigma$), and frontal ($\pm 3\sigma$) views. Reprinted with permission from SZ Li, SC Yan, HJ Zhang, QS Cheng. 2002. Multi-view face alignment using direct appearance models. *Proc 5th Int Conf Automatic Face Gesture Recogn*, pp. 309–314. Copyright ©2002, IEEE.

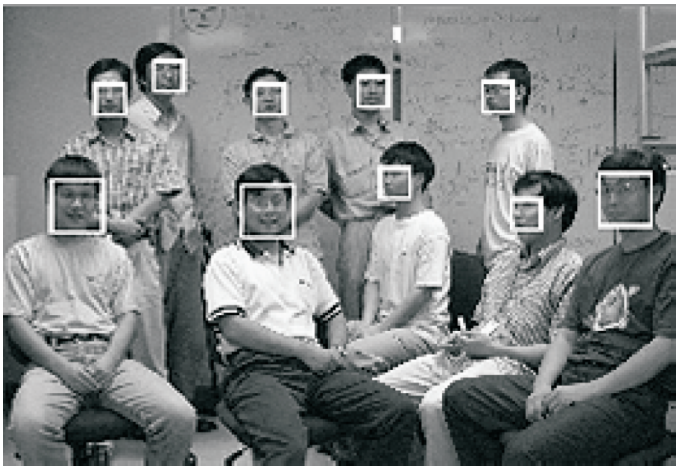

Figure 4. Initial alignment provided by a multi-view face detector. Reprinted with permission from SZ Li, SC Yan, HJ Zhang, QS Cheng. 2002. Multi-view face alignment using direct appearance models. *Proc 5th Int Conf Automatic Face Gesture Recogn*, pp. 309–314. Copyright ©2002, IEEE.

Figure 5. DAM aligned faces (from left to right) at the 0th, 5th, 10th, and 15th iterations, and the original images for (top–bottom) frontal, half-side and full-side view faces. Reprinted with permission from SZ Li, SC Yan, HJ Zhang, QS Cheng. 2002. Multi-view face alignment using direct appearance models. *Proc 5th Int Conf Automatic Face Gesture Recogn*, pp. 309–314. Copyright ©2002, IEEE.

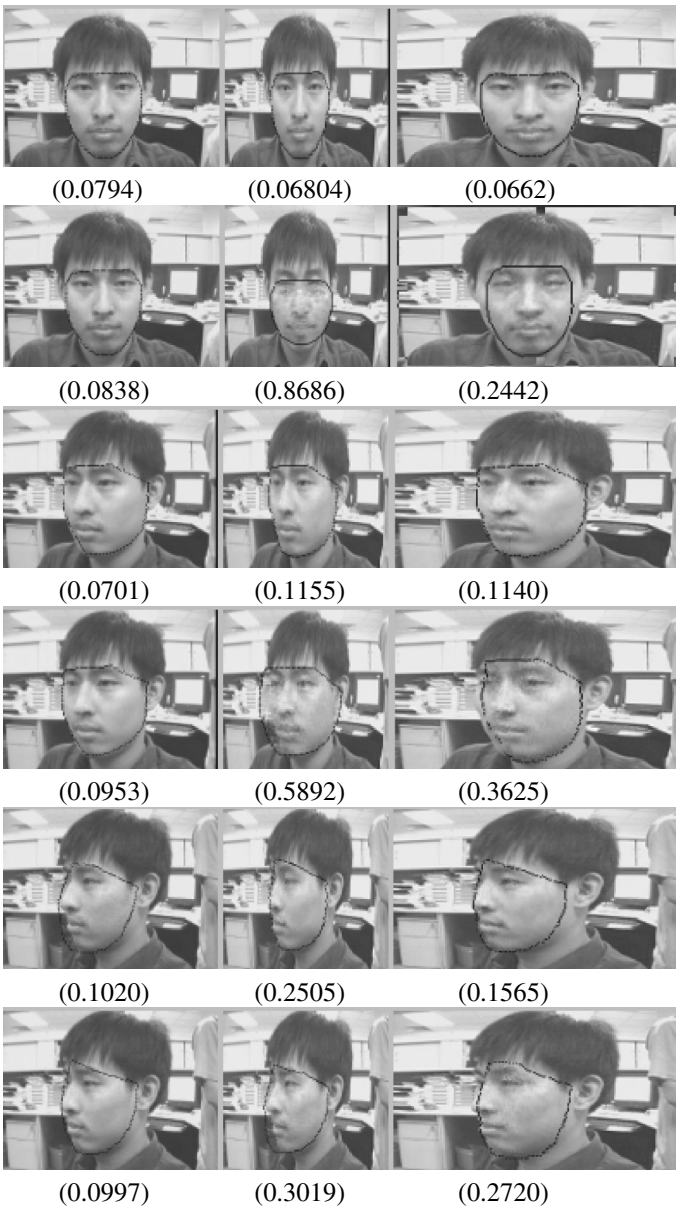

Figure 6. Results of non-isometric (top of each of the three blocks) and isometric (bottom) search for frontal (top block), half-side (middle block), and full-side (bottom block) view faces. From left to right of each row are normal, and stretched faces. The number below each result is the corresponding residual error. Reprinted with permission from SZ Li, SC Yan, HJ Zhang, QS Cheng. 2002. Multi-view face alignment using direct appearance models. *Proc 5th Int Conf Automatic Face Gesture Recogn*, pp. 309–314. Copyright ©2002, IEEE.

Figure 7. Comparison of the manually labeled shape (middle row) and the shape (bottom row) derived from the enclosed texture using the learned projection matrix: $s_t = \mathbf{R}t$. In the top row are the original images. All the images are test data. Reprinted with permission from SC Yan, C Liu, SZ Li, HJ Zhang, H Shum, QS Cheng. 2003. Face alignment using texture-constrained active shape models. *Image Vision Comput* **21**(1):69–75. Copyright ©2003, Elsevier.

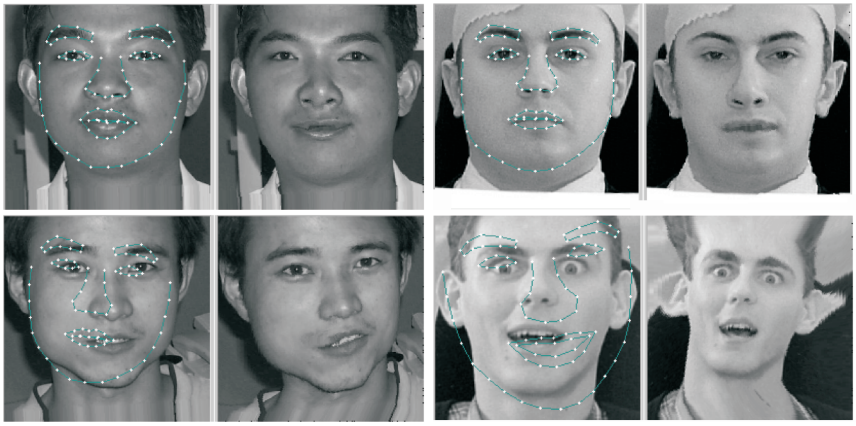

Figure 8. Four face instances of qualified (top) and unqualified (bottom) examples with their warped images. Reprinted with permission from XS Huang, SZ Li, YS Wang. 2004. Statistical learning of evaluation function for ASM/AAM image alignment. In *Proceedings: Biometric Authentication, ECCV 2004 International Workshop, BioAW 2004, Prague, Czech Republic, May 15, 2004* (ECCV Workshop BioAW), pp. 45–56. Ed D Maltoni, AK Jain. New York: Springer. Copyright ©2004, Springer.

---

0. (Input)
   (1) Training examples $\{(x_1, y_1), \ldots, (x_N, y_N)\}$,
   where $N = a + b$; of which a examples have $y_i = +1$
   and b examples have $y_i = -1$;
   (2) The maximum number $M_{\max}$ of weak classifiers to be combined;
1. (Initialization)
   $w_i^{(0)} = \frac{1}{2a}$ for those examples with $y_i = +1$ or
   $w_i^{(0)} = \frac{1}{2b}$ for those examples with $y_i = -1$.
   $M = 0$;
2. (Forward Inclusion)
   while $M < M_{\max}$
   (1) $M \leftarrow M + 1$;
   (2) Choose h_M according to Eq. 36;
   (3) Update $w_i^{(M)} \leftarrow \exp[-y_i H_M(x_i)]$, and normalize to $\sum_i w_i^{(M)} = 1$;
3. (Output)
   $H(x) = \text{sign}[\sum_{m=1}^{M} h_m(x)]$.

Figure 9. AdaBoost algorithm. Reprinted with permission from XS Huang, SZ Li, YS Wang. 2004. Statistical learning of evaluation function for ASM/AAM image alignment. In *Proceedings: Biometric Authentication, ECCV 2004 International Workshop, BioAW 2004, Prague, Czech Republic, May 15, 2004* (ECCV Workshop BioAW), pp. 45–56. Ed D Maltoni, AK Jain. New York: Springer. Copyright ©2004, Springer.

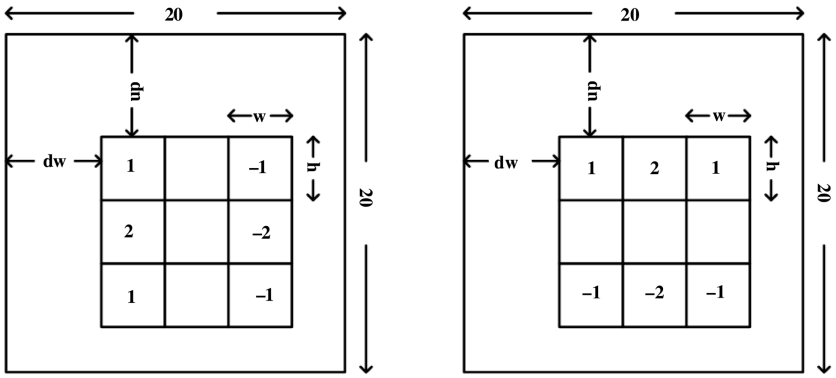

Figure 10. The two types of simple Sobel-like filters defined on sub-windows. The rectangles are of size $w \times h$ and are at distances of (dw, dh) apart. Each feature takes a value calculated by the weighted $(\pm 1, \pm 2)$ sum of the pixels in the rectangles. Reprinted with permission from XS Huang, SZ Li, YS Wang. 2004. Statistical learning of evaluation function for ASM/AAM image alignment. In *Proceedings: Biometric Authentication, ECCV 2004 International Workshop, BioAW 2004, Prague, Czech Republic, May 15, 2004* (ECCV Workshop BioAW), pp. 45–56. Ed D Maltoni, AK Jain. New York: Springer. Copyright ©2004, Springer.

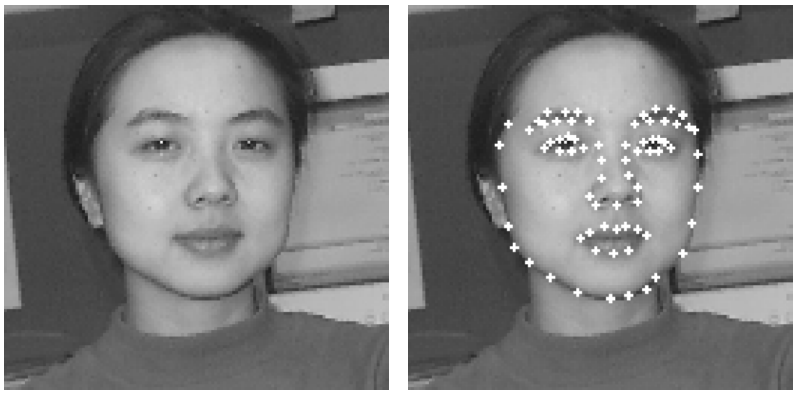

Figure 11. A face image and the landmark points. Reprinted with permission from XW Hou, SZ Li, HJ Zhang, QS Cheng. 2001. Direct appearance models. *Proc IEEE Conf Comput Vision Pattern Recogn* **1**:828–833. Copyright ©2001, IEEE.

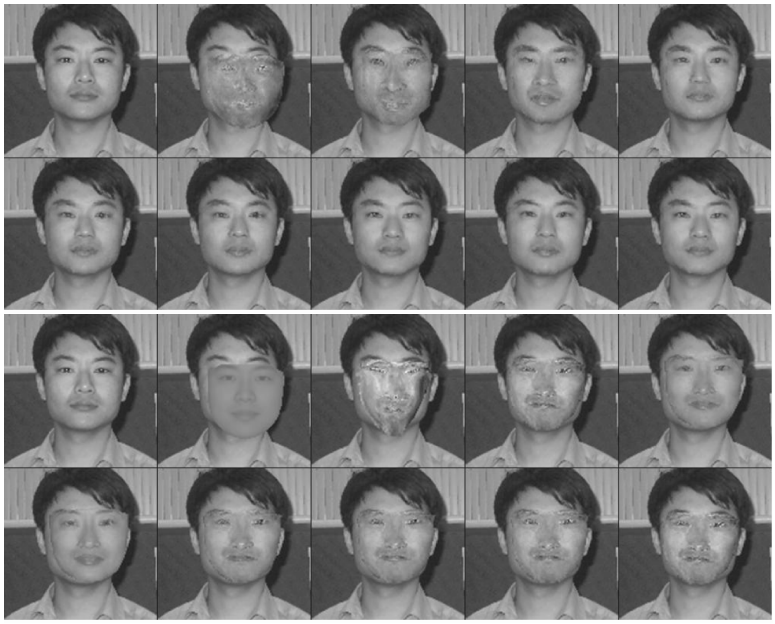

Figure 12. Scenarios of DAM (top) and AAM (bottom) alignment. Reprinted with permission from XW Hou, SZ Li, HJ Zhang, QS Cheng. 2001. Direct appearance models. *Proc IEEE Conf Comput Vision Pattern Recogn* **1**:828–833. Copyright ©2001, IEEE.

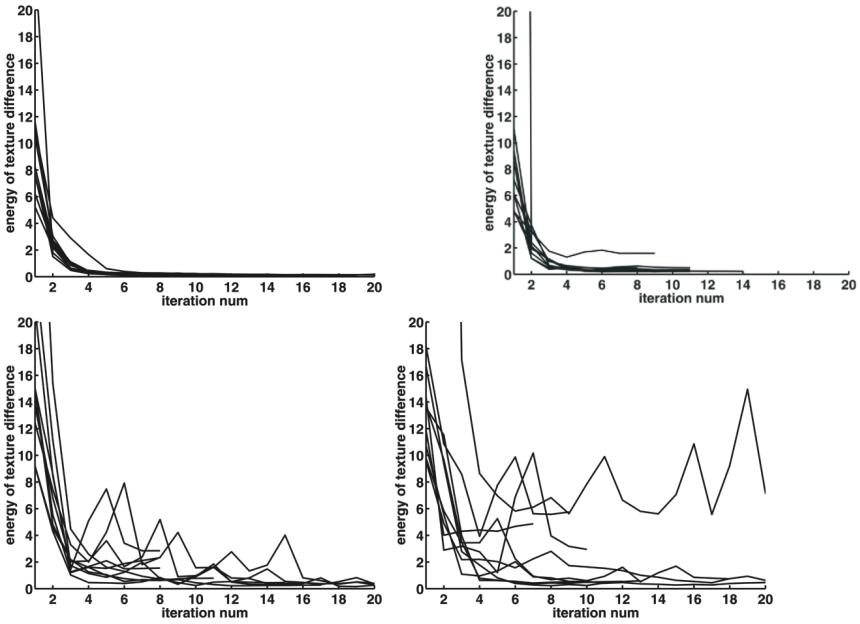

Figure 13. The evolution of total δT for the DAM (top) and AAM (bottom) as a function of iteration number for the training (left) and test (right) images. Reprinted with permission from XW Hou, SZ Li, HJ Zhang, QS Cheng. 2001. Direct appearance models. *Proc IEEE Conf Comput Vision Pattern Recogn* **1**:828–833. Copyright ©2001, IEEE.

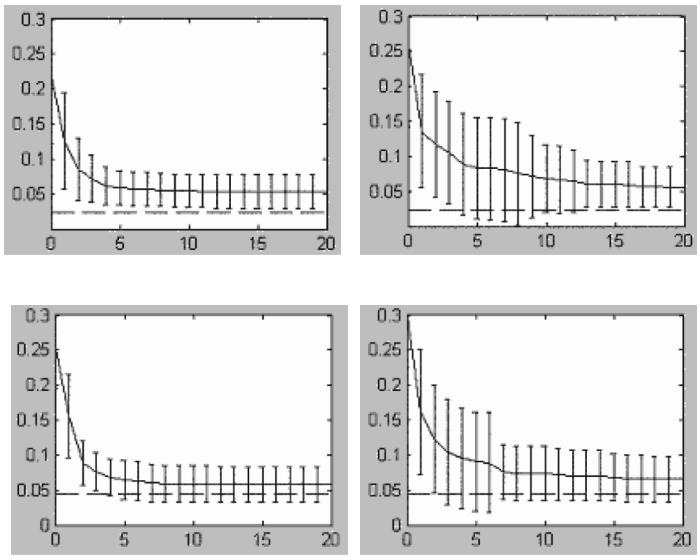

Figure 14. Mean error (the curve) and standard deviation (the bars) in reconstructed texture $\|\delta T\|$ as a function of iteration number for DAM (left) and AAM (right) methods with the training (top) and test (bottom) sets, for frontal face images. The horizontal dashed lines in the lower part of the figures indicate average $\|\delta T\|$ for the manually labeled alignment. Reprinted with permission from SZ Li, SC Yan, HJ Zhang, QS Cheng. 2002. Multi-view face alignment using direct appearance models. *Proc 5th Int Conf Automatic Face Gesture Recogn*, pp. 309–314. Copyright ©2002, IEEE.

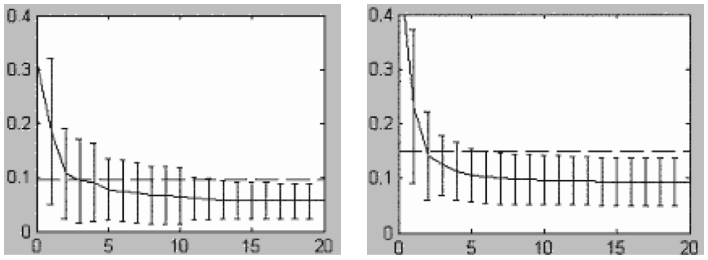

Figure 15. Mean error in $\|\delta T\|$ and standard deviation of DAM alignment for half- (left) and full- (right) side view face images from the test set. Note that the mean errors in the calculated solutions are smaller than obtained using the manually labeled alignment after a few iterations. Reprinted with permission from SZ Li, SC Yan, HJ Zhang, QS Cheng. 2002. Multi-view face alignment using direct appearance models. *Proc 5th Int Conf Automatic Face Gesture Recogn*, pp. 309–314. Copyright ©2002, IEEE.

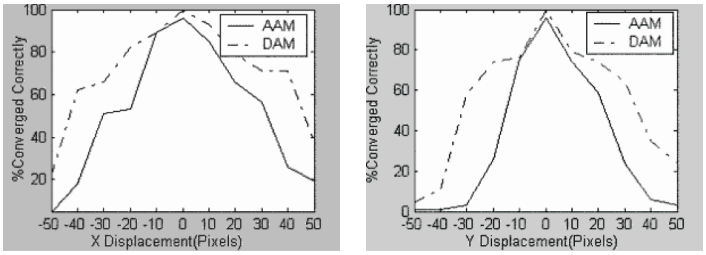

Figure 16. Alignment accuracy of the DAM (dashed) and AAM (solid) in terms of localization errors in the x (left) and y (right) directions. Reprinted with permission from SZ Li, SC Yan, HJ Zhang, QS Cheng. 2002. Multi-view face alignment using direct appearance models. *Proc 5th Int Conf Automatic Face Gesture Recogn*, pp. 309–314. Copyright ©2002, IEEE.

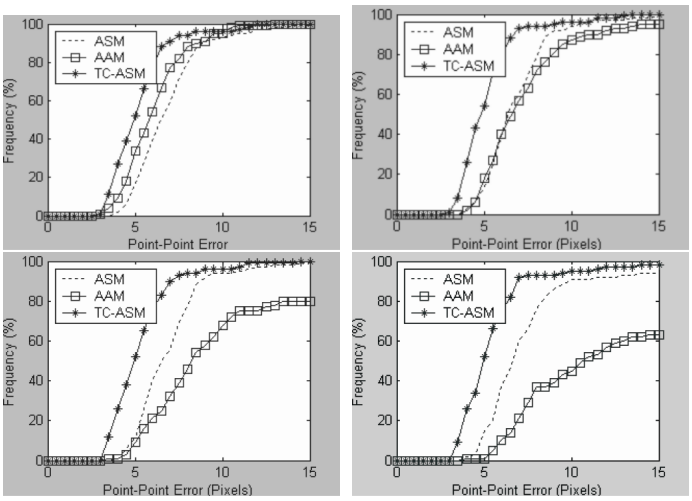

Figure 17. Accuracy of ASM, AAM, TC-ASM. From upper to lower, left to right, are the results obtained with the initial displacements of 10, 20, 30, and 40 pixels. Note that the value of the vertical coordinate is the percentage of examples that have the point-to-point distance smaller than the corresponding value of horizonal coordinate. Reprinted with permission from SC Yan, C Liu, SZ Li, HJ Zhang, H Shum, QS Cheng. 2003. Face alignment using texture-constrained active shape models. *Image Vision Comput* **21**(1):69–75. Copyright ©2003, Elsevier.

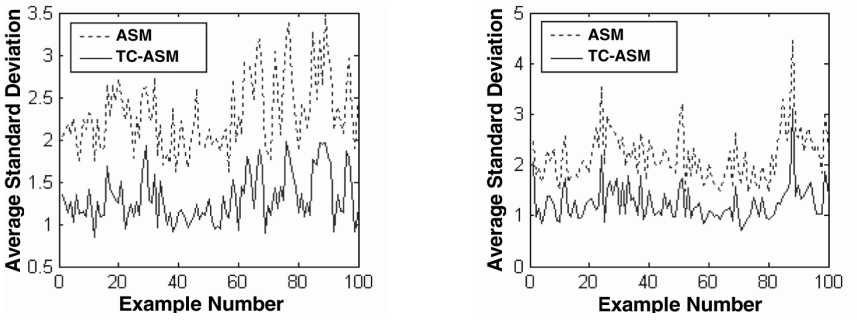

Figure 18. Standard deviation in the results of each example for ASM (dotted) and TC-ASM (solid) with the training set (left) and the test set (right). Reprinted with permission from SC Yan, C Liu, SZ Li, HJ Zhang, H Shum, QS Cheng. 2003. Face alignment using texture-constrained active shape models. *Image Vision Comput* **21**(1):69–75. Copyright ©2003, Elsevier.

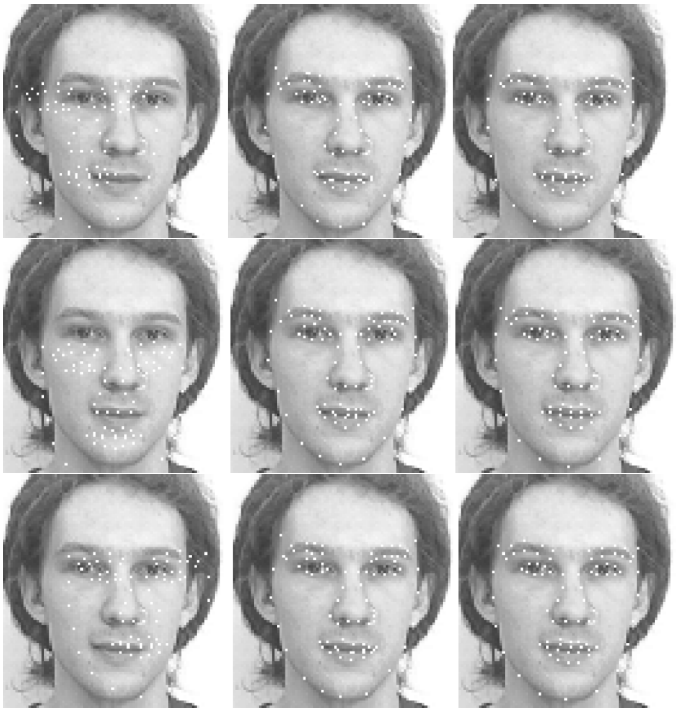

Figure 19. Stability of the ASM (middle column) and the TC-ASM (right column) in shape localization. The different initialization conditions are shown in the left column. Reprinted with permission from SC Yan, C Liu, SZ Li, HJ Zhang, H Shum, QS Cheng. 2003. Face alignment using texture-constrained active shape models. *Image Vision Comput* **21**(1):69–75. Copyright ©2003, Elsevier.

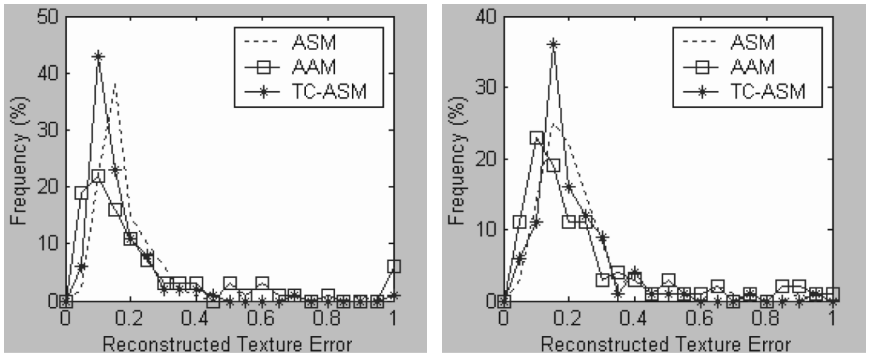

Figure 20. Distribution of the texture reconstruction error with the ASM (dotted), the AAM (square), and the TC-ASM (asterisk), with training data (left) and test data (right). Reprinted with permission from SC Yan, C Liu, SZ Li, HJ Zhang, H Shum, QS Cheng. 2003. Face alignment using texture-constrained active shape models. *Image Vision Comput* **21**(1):69–75. Copyright ©2003, Elsevier.

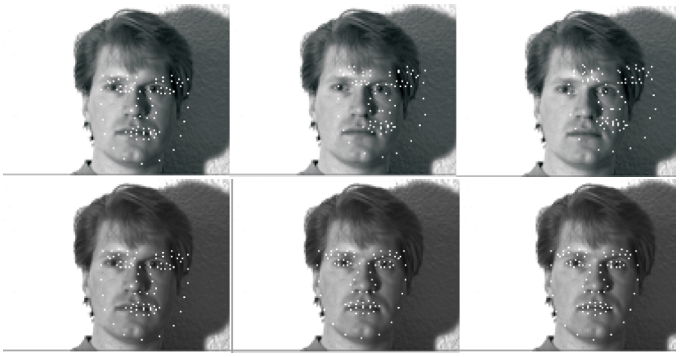

Figure 21. Sensitivities of the AAM (upper) and TC-ASM (lower) to an illumination condition not seen in the training data. From left to right are the results obtained at the 0th, 2th, and 10th iterations. Result in different levels of image pyramid is scaled back to the original scale. Reprinted with permission from SC Yan, C Liu, SZ Li, HJ Zhang, H Shum, QS Cheng. 2003. Face alignment using texture-constrained active shape models. *Image Vision Comput* **21**(1):69–75. Copyright ©2003, Elsevier.

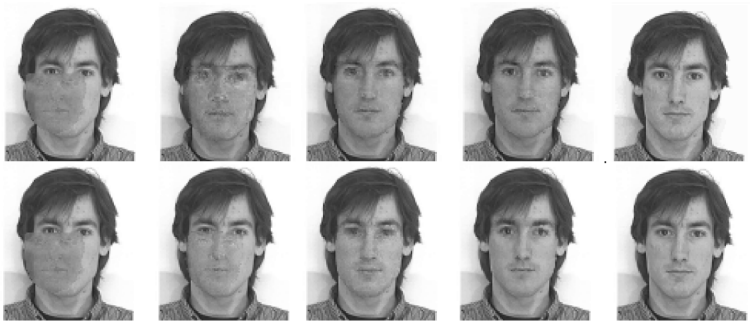

Figure 22. Scenarios of AAM (upper) and TC-ASM (lower) alignment with texture reconstruct errors 0.3405 and 0.1827, respectively. From left to right are the results obtained at the 0th, 5th, 10th, and 15th iterations, and the original image. Result in different levels of image pyramid is scaled back to the original scale. Reprinted with permission from SC Yan, C Liu, SZ Li, HJ Zhang, H Shum, QS Cheng. 2003. Face alignment using texture-constrained active shape models. *Image Vision Comput* **21**(1):69–75. Copyright ©2003, Elsevier.

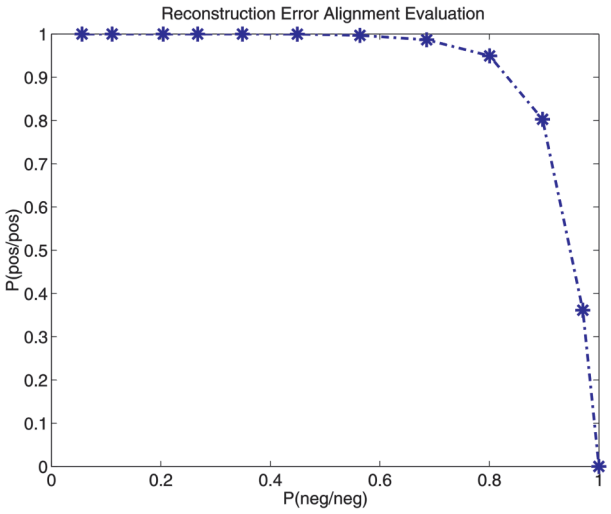

Figure 23. ROC curve for the reconstruction error-based alignment evaluation for the training set. Reprinted with permission from XS Huang, SZ Li, YS Wang. 2004. Statistical learning of evaluation function for ASM/AAM image alignment. In *Proceedings: Biometric Authentication, ECCV 2004 International Workshop, BioAW 2004, Prague, Czech Republic, May 15, 2004* (ECCV Workshop BioAW), pp. 45–56. Ed D Maltoni, AK Jain. New York: Springer. Copyright ©2004, Springer.

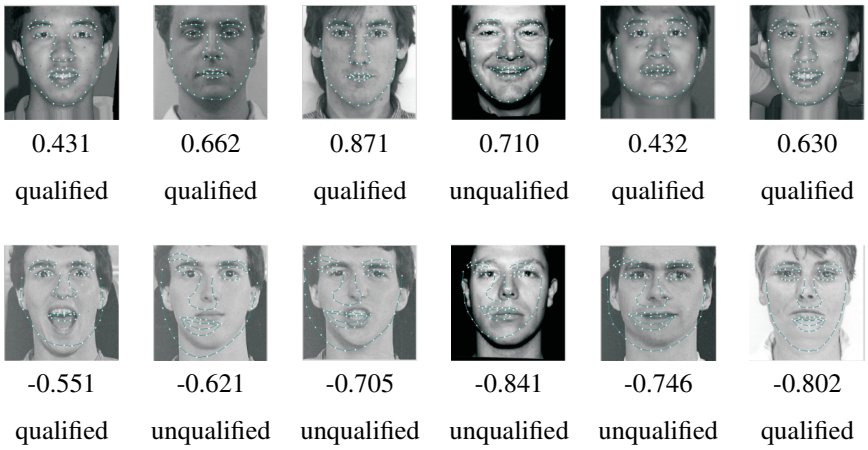

Figure 24. Alignment quality evaluation results: accepted images (top) and rejected images (bottom). Reprinted with permission from XS Huang, SZ Li, YS Wang. 2004. Statistical learning of evaluation function for ASM/AAM image alignment. In *Proceedings: Biometric Authentication*, ECCV 2004 International Workshop, BioAW 2004, Prague, Czech Republic, May 15, 2004 (ECCV Workshop BioAW), pp. 45–56. Ed D Maltoni, AK Jain. New York: Springer. Copyright ©2004, Springer.

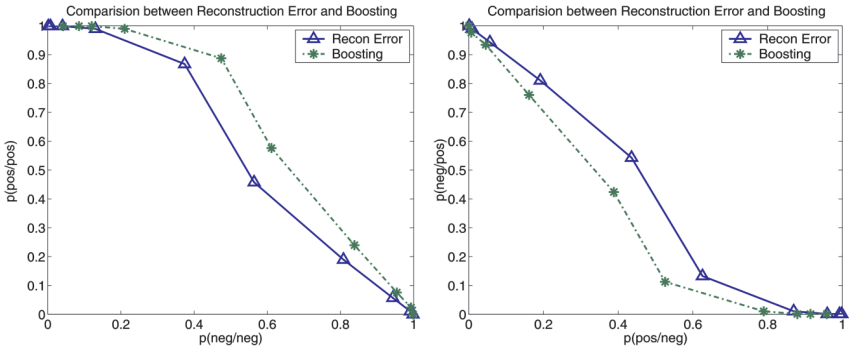

Figure 25. Comparison between reconstruction error method and boost method. Reprinted with permission from XS Huang, SZ Li, YS Wang. 2004. Statistical learning of evaluation function for ASM/AAM image alignment. In *Proceedings: Biometric Authentication, ECCV 2004 International Workshop, BioAW 2004, Prague, Czech Republic, May 15, 2004* (ECCV Workshop BioAW), pp. 45–56. Ed D Maltoni, AK Jain. New York: Springer. Copyright ©2004, Springer.